Polymorphic Associations and Structures of the Cross-Seeding of Aβ$_{1−42}$ and hIAPP$_{1−37}$ Polypeptides

Mingzhen Zhang,[†] Rundong Hu,[†] Hong Chen,[†] Xiong Gong,[‡] Feimeng Zhou,[§] Li Zhang,[∥] and Jie Zheng[*,†]

[†]Department of Chemical and Biomolecular Engineering and [‡]College of Polymer Science and Polymer Engineering, The University of Akron, Akron, Ohio 44325, United States

[§]Department of Chemistry and Biochemistry, California State University, Los Angeles, Los Angeles, California 90032, United States

[∥]Department of Geriatric Neurology, Nanjing Brain Hospital Affiliated to Nanjing Medical University, Nanjing, Jiangsu 210029, China

ABSTRACT: Emerging evidence have shown that the patients with Alzheimer's disease (AD) often have a higher risk of later developing type II diabetes (T2D), and vice versa, suggesting a potential pathological link between AD and T2D. Amyloid-β (Aβ) and human islet amyloid polypeptide (hIAPP) are the principle causative components responsible for the pathologies of AD and T2D, respectively. The cross-sequence interactions between Aβ and hIAPP may provide a molecular basis for better understanding the potential link between AD and T2D. Herein, we systematically modeled and simulated the cross-sequence aggregation process, molecular interactions, and polymorphic structures of full-length Aβ and hIAPP peptides using a combination of coarse-grained (CG) replica-exchange molecular dynamics (REMD) and all-atom molecular dynamics (MD) simulations, with particular focus on the effect of association models between Aβ and hIAPP on the structural stability and polymorphic populations of hybrid Aβ−hIAPP aggregates. Four distinct association models (double-layer, elongation, tail−tail, and block models) between Aβ and hIAPP oligomers were identified, and the associated polymorphic Aβ−hIAPP structures were determined as well. Among them, different association models led to different Aβ−hIAPP aggregates, with large differences in structural morphologies and populations, interacting interfaces, and underlying association forces. The computational models support the cross-sequence interactions between Aβ and hIAPP pentamers, which would lead to the complex hybrid Aβ−hIAPP assemblies. This computational work may also provide a different point of view to a better understanding of a potential link between AD and T2D.
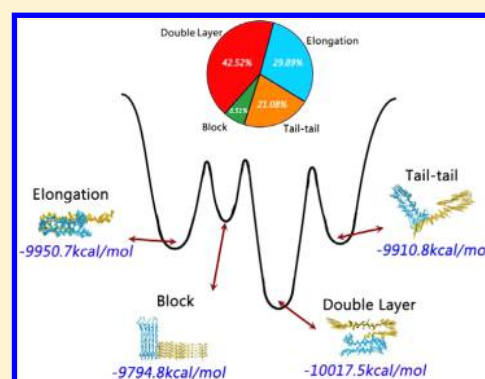
INTRODUCTION

Misfolding and aggregation of homoamyloid peptides into small oligomers and mature amyloid fibers are often associated with the pathological features of many neurodegenerative diseases, such as Alzheimer disease (AD),[1,2] type II diabetes (T2D),[3−5] Huntington's disease,[6] and Parkinson's disease.[2,7] Significant efforts have been made to study the conformational conversion/aggregation, toxicity, and inhibition of homoamyloid peptides.[8−12] It is generally believed that under disease conditions, soluble amyloid oligomers are more neuron toxic than mature fibrils.[13] Amyloid oligomers are highly polymorphic with different sizes, conformations, and morphologies, and they all contain some aggregates with certain degrees of β-sheet structures.[10,14−16] Recently, more biologically importantly and interesting findings have reported that different amyloid peptides can interact with each other to form hybrid amyloids containing conformationally cross-β-sheet structures similar to homoamyloids.[17−21] Typical examples of these hybrid amyloids were comprised of β-amyloid (Aβ)−islet amyloid peptides (IAPP), Aβ−tau, Aβ−prion, human IAPP−rat IAPP, and tau−

synuclein amyloids.[22−36] These important findings imply a potential pathological link between different amyloid diseases.[37]

Specifically, AD and T2D are the most common amyloid disorders. Clinical and epidemiological evidence have shown that the patients with T2D often have a higher risk of later developing Alzheimer's and vice versa.[38−40] Although Aβ and hIAPP—the principle components of amyloid deposits for AD and T2D, respectively—involve different secretory pathways, they also share many structural and functional similarities during the aggregation process.[22,41] Under disease conditions, both Aβ and hIAPP undergo similar structural conversion and aggregation from disordered monomers to β-sheet-rich aggregates, which will impair the surrounding tissues, activate the proinflammatory responses, and eventually lead to neurodegeneration.[42−44] Many mechanisms have been proposed to interpret the toxicity of Aβ and hIAPP amyloid aggregates.[7,45] Accumulating evidence appears to support that Aβ and hIAPP aggregates achieve their toxicity to target cells by

disrupting cell membranes and membrane functions.[5,46−49] Although the exact molecular link between AD and T2D is still unclear, those common structural characteristics and biological response suggest a potential link between AD and T2D, which may occur as a result of the complex ways, i.e. Aβ and hIAPP interact with each other to produce toxic, hybrid Aβ−hIAPP aggregates, which damages brain cells and adipose tissue to use sugar and respond to insulin.

Several lines of evidence appear to support the hypothesis of cross-sequence interaction between Aβ and hIAPP: (i) Aβ and hIAPP were found to coexist in the serum and cerebrospinal fluids with similar concentrations;[41] (ii) IAPP, normally cosecreted with insulin, can also be expressed by the sensory neurons and has the high affinity binding sites at hind-brain;[50−52] (iii) Aβ was found to colocalize with hIAPP in pancreatic islet amyloid deposits of T2D patients;[53] (iv) Aβ and hIAPP, possessing 38% sequence similarity, have been demonstrated to interact with each other to form hybrid amyloid fibrils in vitro.[39,41] However, it is still unclear how Aβ and hIAPP interact with each other and how their interactions impact the aggregation kinetics and structures of hybrid amyloid formation. Due to the fast kinetics of amyloid aggregation, it is experimentally challenging to characterize any pure oligomer at molecular level. The aggregation scenario and structural characterization are further complicated when considering cross-sequence interactions between different Aβ and hIAPP peptides. This further emphasizes the importance of understanding of the cross-sequence interaction between Aβ and hIAPP.

In this work, we performed a multiscale simulation platform combining coarse-grained and all-atom molecular dynamics (MD) simulations to systematically investigate the aggregation process of full-length Aβ and hIAPP pentamers and to determine different aggregated Aβ−hIAPP structures. Using the coarse-gained replica-exchange MD (REMD) simulations, we first determined four hybrid Aβ−hIAPP aggregates at the lowest energy states, followed by the structural refinement and validation by explicit-solvent all-atom MD simulations. All the Aβ−hIAPP aggregates were identified to be structurally stable with well conserved secondary structures and interacting interfaces. On the basis of different association interfaces between hIAPP and Aβ pentamers, the Aβ−hIAPP decamers were further classified into four different interaction modes of double-layer, elongation, tail−tail, and block modes. Different Aβ−hIAPP interaction modes presented different cross-seeding pathways and structures of Aβ and hIAPP, which may affect (accelerate, delay, or block) amyloid propagation of both pure and hybrid amyloid peptides. The findings from our long simulations (up to ∼20 μs) provide the atomic-level structural details of Aβ−hIAPP cross-seeding aggregates and help understand a potential molecular connection between AD and T2D.

■ MATERIALS AND METHODS

hIAPP$_{1−37}$ and A$\beta_{1−42}$ Models. In this work, the initial all-atom coordinates for hIAPP$_{1−37}$ and A$\beta_{1−42}$ monomer were obtained from the NMR structures by Tycko's and Riek's laboratories.[54,55] Because of the polymorphic nature of amyloid peptides, many distinctive structural models of Aβ have been proposed and determined under different experimental conditions and using different crystallization methods, including the triple three-β-sheet A$\beta_{1−42}$ model by Xiao et al.,[56] the U-bend-shaped structures of A$\beta_{1−42}$ by Ahmed et al.,[57] and the

double-layer and triple-layer A$\beta_{1−40}$ models by Tycko et al.[58,59] Despite of their structural differences, the residues in full-length Aβ assemblies employed the parallel β-sheet-like structures. Here we applied the Riek model to construct Aβ pentamer, and the missing residues 1−16 of A$\beta_{1−42}$ (PDB: 2BEG) were added in the in-register manner with the β-sheet conformation as suggested by Miller et al.[60] There was no specific PDB ID available for hIAPP$_{1−37}$, but the Tycko lab provided us hIAPP$_{1−37}$ NMR structures upon our request. For both hIAPP$_{1−37}$ and A$\beta_{1−42}$ peptides, each monomer maintained a U-bend conformation with two antiparallel β-sheet strands bridged by the turn region. A number of experimental and computational studies have showed that have demonstrated that hIAPP$_{1−37}$ and A$\beta_{1−42}$ pentamers with a U-bend conformation exhibits high structural stability and serves as a basic template nucleus for amyloid growth via either monomer attachment for elongation or lateral stacking.[57,61−65] Moreover, small amyloid oligomers such as pentamer and hexamer are the most abundant soluble oligomers, and their toxicity is one of the highest.[66] To construct an all-atom Aβ or hIAPP pentamer, five Aβ or hIAPP monomers were parallel packed on top of each other in an in-register manner with an interpeptide distance of ∼4.7 Å. Each all-atom hIAPP and Aβ pentamer was solvated in the water box with NaCl concentrations of 0.15 M, and then simulated for 100 ns to achieve the equilibrate state in the NPT ensemble using the Gromacs-4.6.5 program. Then, the resulting equilibrated all-atom Aβ and hIAPP pentamers were converted into coarse-grained (CG) models by the elastic network potential of the Martini force field (version 2.4),[67] which will be used for studying the cross-sequence aggregation and interactions between Aβ and hIAPP pentamers by CG-REMD simulations.

Hybrid Aβ−hIAPP Assemblies. Hybrid Aβ−hIAPP assemblies were obtained from the CG-based REMD trajectories at 310 K using an in-house cluster analysis. Briefly, the free energy landscape that describes the interaction between hIAPP and Aβ were constructed using $-RT \log(H(x, y))$, where $H(x, y)$ is the histogram of two selected reaction coordinates: x is root-mean-square derivation (RMSD) and x and y are the radius of gyration (R_g). Based on the free energy landscape, the four most populated CG Aβ−hIAPP hetero-assemblies (double-layer, elongation, tail−tail, and block modes) were identified at different energy potential wells.

Conversion of CG-REMD Models to All-Atom Structures. Our strategy for obtaining all-atom representation from CG coordinate set is similar to the method described previously for the reverse coarse-graining of self-assembly of lipids into micelles.[68] Given the predefined CG-residue models by Gromacs, the first stage of backmapping is the generation of an initial, all-atom structure. We first used the center of mass of the group of atoms represented by a single CG bead as the center of mass location of backbones (Bcom), side chains (Scom), and/or other peripheral groups (Pcom) for each residue. Considering that the secondary structures of CG models do not experience a large conformational change, we then used the previously determined all-atom structures of hIAPP or Aβ as a template and roughly placed the center of mass of all-atom backbones, side chains, and/or peripheral groups on the interpolated positions of Bcom, Scom, and/or Pcom for each residue of the same hIAPP or Aβ peptides. So, all atoms were assigned coordinates according to standard geometries using GROMACS around these mapped atoms. The resulting structure was then optimized by energy

minimization to remove any bad contact and to correct internal coordinates for all bonded atoms. The second stage is the optimization of interfacial contacts between Aβ and hIAPP. The resulting all-atom structure obtained from the first stage was further recast into the initial all-atom Aβ or hIAPP models to maximize residue–residue contacts by minor structural adjustments through structural superimposition and rotation, followed by energy minimization to obtain a starting structure for further simulation. In this way, the structural disorder of the resulting all-atom structures, caused by the high temperatures in CG-based REMD simulation, was minimized. We will provide our backmapping script written by TCL upon request.

All-Atom MD Simulations. All explicit-solvent all-atom simulations were conducted using the Gromacs-4.6.5 program with the CHARMM27 force field with CMAP correction and the SPCE solvent models.[69,70] All systems were solvated in the cubic water box with minimal margin of 15 Å from any protein atom to any edge of water box. Cl$^-$ and Na$^+$ ions were added into the systems to mimic ~150 mM ionic strength. The resulting systems were structurally optimized and relaxed by 50 000 steps of the steepest decent minimization. The energy minimized systems were gradually heated from 0 to 310 K by 1 ns MD simulations with constraining the peptide backbones. MD simulations were conducted for 60 ns using the NPT ensemble ($T = 310$ K and $P = 1$ atm) and under periodic boundary conditions. The Parrinello–Rahman and the V-rescale methods were used to maintain a constant pressure of 1 atm and temperature of 310 K, respectively. The protein and solvent were separately coupled to external temperature and pressure baths. All covalent bonds involving hydrogen atoms were constrained by the LINCS method. Short-range van der Waals (VDW) interactions were described by the smoothly truncated method via potential shift at 14 Å. Long-range electrostatic interactions were calculated by the particle mesh Ewald (PME) method with a grid spacing of 0.16 Å and a real-space cutoff of 12 Å. The equations of motion were integrated using the Leapfrog integrator with a time-step of 2 fs. Structures were saved every 2 ps for analysis. All analyses were performed using the tools within the CHARMM, VMD, and in-house codes.

CG-REMD Simulations. In this work, the conformational sampling and association of Aβ and hIAPP pentamers were performed using the CG-REMD simulations with Gromacs-4.6.5 software package, which has been demonstrated as one of the most efficiency sampling methods, particularly suitable for the study of protein folding, aggregation, and self-assembly processes.[69,71] Here, a total of 40 independent replicas with the temperatures (306.88, 309.21, 311.54, 313.90, 316.26, 318.64, 321.04, 323.44, 325.87, 328.30, 330.76, 333.22, 335.70, 338.20, 340.71, 343.21, 345.78, 348.33, 350.90, 353.49, 356.09, 358.72, 361.35, 364.00, 366.66, 369.34, 372.04, 374.75, 377.48, 380.23, 382.99, 385.77, 388.56, 391.41, 394.24, 397.08, 399.95, 402.83, 405.73, and 408.65 K) were simulated simultaneously for each system. Each replica contains a CG hIAPP and Aβ pentamer that were separated from each other by ~40 Å with random orientations. Such structural arraignment allows to avoid any potential artificial effect on the aggregation process of Aβ and hIAPP. Based on the fitted energy–temperature curve and the Metropolis criterion, the acceptance ratio varies between 0.20 and 0.25. With the potential-shift modifier, a cutoff of 1.2 nm was used for the nonbond interactions. The shift method was used to describe the long-range electrostatics interactions. The temperatures and pressure (1 atm) were controlled by the V-

rescale and Parrinello–Rahman methods with the coupling constants of 1.0 and 12.0 ps, respectively. The temperature coupling was conducted separately for the protein and nonprotein atoms (i.e., ions and water molecules). Leapfrog integrator was utilized to allow an integration time step of 4 fs. Among different time-steps of 30, 20, 10, 8, and 4 fs being tested in the CG-simulations, we found that 4 fs is the best for the elastic network model, which can well maintain the integrity of Aβ and hIAPP pentamers and eliminate their structural disturbance at the high temperatures induced by REMD simulations. The exchange between two replicas was attempted every 1000 integration steps. For each replica, the simulation time was 500 ns.

Conformer Population Analysis. To further obtain insights into the relative population distributions of four representative Aβ–hIAPP assemblies, we extracted 500 structures per each assembly model from the last 10 ns explicit-water MD trajectories, with excluding water molecules. A total of 500 × 4 = 2000 Aβ–hIAPP conformers were then used to create an energy landscape of Aβ–hIAPP assemblies for evaluating the probability of conformers using an in-house Monte Carlo program as reported in our previous studies.[25,72,73] To reduce thermal fluctuations induced by MD simulations, all conformers were energy minimized by 400 steps of the ABNR algorithm, and the conformation energies of all conformers were calculated using generalized Born method with molecular volume (GBMV), generating a Markov chain of all conformers $[E_1, E_2, ..., E_i, ..., E_n]$. For conformer population analysis, any two structures from conformers i and j were randomly selected and their conformational energies were calculated using the GBMV model. Then, metropolis algorithm was applied to determine the transition probability (i.e., acceptance probability) from conformer i to conformer j using $P_{accept,move} = \min[1, \exp((E_i - E_j)/k_B T)]$. After 1 million step samplings, a total number of "accepted" structures (N_i) for any conformer i was counted, and the relative probability of conformer i occurring in the energy landscape was evaluated as $p_i = N_i/N_{total}$.

■ RESULTS AND DISCUSSION

Numerous computational studies have reported different atomic-resolution structures of Aβ and hIAPP oligomers/fibrils alone and the misfolding process of Aβ and hIAPP using all-atom MD simulations or CG simulations or both.[74] However, with current computational power and resource, it is extremely challenging or infeasible to directly simulate the misfolding and aggregation process of heterogeneous amyloid peptides of Aβ and hIAPP, with both peptides starting from unfolded random structures to well-folded cross-β-sheet structures. Such simulations usually require at least ms+ time scale, which is beyond the scope of this work. In this work, we performed a hybrid multiresolution simulation platform to study the aggregate process of the folded Aβ and hIAPP oligomers and their aggregated Aβ–hIAPP structures by combining the efficiency of the CG model with the accuracy of the all-atom model. Our hIAPP–rIAPP heteroassemblies were constructed based on our recent experimental observations (unpolished data): (1) our AFM and ThT experiments have shown that Aβ and hIAPP can associate with each other to form hybrid amyloid oligomers and fibrils and (2) The NMR structures of Aβ and hIAPP fibrils provide a structural basis for building our models. Our previous MD simulations on pure Aβ and hIAPP oligomers were also able to largely reproduce NMR-derived

structures.[25,61,75,76] Figure 1 shows a flowchart of the performed work. (1) We first constructed all-atom Aβ and hIAPP
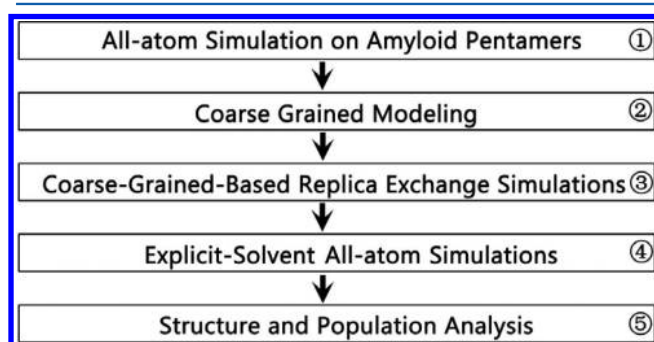

Figure 1. General simulation flowchart.

pentamers with a U-bend conformation, followed by explicit-solvent all-atom MD simulations (100 ns) to obtain the equilibrium structures of Aβ and hIAPP pentamers separately. Aβ and hIAPP pentamers were chosen because previous studies have identified both Aβ and hIAPP pentamers as one of the most populated oligomeric species, which may serve as initial seeds for amyloid propagation.[61] (2) Upon obtaining all-atom Aβ and hIAPP pentamers at the equilibrium state, we converted them into the CG-based Aβ and hIAPP pentamers with well-preserved U-bend conformation using the Martini force field (version 2.4). The MARTINI CG model is a general force field for peptides and other molecules that has often been used to describe self-assembly in solution and in lipid membranes while still preserving the physical and chemical properties of a determined molecular system after averaging key aspects of the atomistic details.[77] (3) We applied the replica-exchange MD simulations (20 μs) to study the cross-species aggregation process of Aβ and hIAPP pentamers in the CG representations. (4) We determined the most possible Aβ−hIAPP aggregates at the local lowest energy states from the free energy landscape of CG-REMD simulations, and these CG Aβ−hIAPP aggregates were then converted back to all-atom structures, followed by structural validation by explicit-solvent all-atom MD simulations (240 ns). (5) Finally, conformer population analysis of different all-atom Aβ−hIAPP aggregates was performed to determine polymorphic and thermodynamic properties of hybrid Aβ−hIAPP aggregates. All the simulation systems are summarized in Table 1.

All-Atom Structures of hIAPP and Aβ Pentamers. A number of experimental and computational studies have shown

Table 1. Summary of the All-Atom Simulation Systems of Pure Aβ, Pure hIAPP, and Hybrid Oligomers[a]

system	RMSD (Å)	SASA (Å²)	time (ns)
hIAPP pentamer	6.3 ± 0.9	10322.6 ± 174.2	100
Aβ pentamer	10.6 ± 1.3	13254.9 ± 131.5	100
double-layer Aβ−hIAPP decamer	5.4 ± 0.8	20180.9 ± 245.1	60
elongation Aβ−hIAPP decamer	5.5 ± 0.8	20622.1 ± 249.0	60
tail−tail Aβ−hIAPP decamer	8.1 ± 1.4	21376.8 ± 262.2	60
block Aβ−hIAPP decamer	10.0 ± 1.7	23305.8 ± 308.0	60

[a]RMSDs and SASAs are calculated from the last 10 ns trajectories for each system.

that Aβ and hIAPP pentamers are the more stable, small oligomers, which often act as nucleation seeds for forming higher-order amyloid aggregates.[61] Here, we first built Aβ and hIAPP pentamers separately, and each pentamer contained five peptides with a U-bend cross-β-sheet conformation and with a parallel in-registered packing. The U-bend conformation resembles the corresponding fibril structures of Aβ and hIAPP, as derived from solid-state NMR.[54,55] Then, we carried out 100 ns all-atom MD simulations for both Aβ and hIAPP pentamers in explicit water at 310 K. Figure 2 shows the
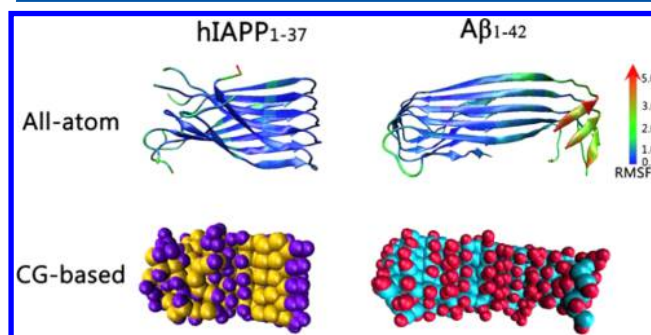

Figure 2. All-atom and CG-based structures of hIAPP and Aβ pentamers. In all-atom models, RMSF values imposed on each residue are denoted by a blue (small RMSF) to red (large RMSF) color scale.

averaged structures of hIAPP and Aβ pentamers obtained from the last 10 ns trajectories (upper panel), where the root-mean-square fluctuation (RMSF) values were imposed on each residue in a blue-to-red color scale. Visual inspection of MD trajectories revealed that during the 100 ns simulations, two pentamers showed high structural stability with well-preserved U-bend conformations and without any disassociation tendency between peptides. Quantitatively, small conformational changes of both Aβ and hIAPP pentamers were observed, as reflected by stabilized root-mean-square deviations (RMSDs) (RMSD$_{Aβ}$ = 10.61 ± 1.34 and RMSD$_{hIAPP}$ = 6.37 ± 0.97 Å). Aβ and hIAPP pentamers also retained high β-sheet contents of 50.4% and 47.9%, respectively. RMSF data showed that residues in the β-strand regions exhibited a much lower flexibility than those in the turn region and near the N-/C-terminus where small peptide twists occurred in the terminal regions. Taken together, all-atom Aβ and hIAPP pentamers exhibited high structural stability, consistent with previous studies,[61,75] so they can be used as initial structural templates for constructing the corresponding CG structures of Aβ and hIAPP pentamers.

Hybrid Aβ−hIAPP Assemblies by CG-REMD Simulations. In Figure 2, we converted the all-atom structures of Aβ and hIAPP pentamers into the CG structures of Aβ and hIAPP pentamers using the elastic network method with the Martini force fields (version 2.4, low panel). Due to the limited structure and kinetic information about the cross-sequence interaction and aggregation between Aβ and hIAPP oligomers, we applied CG-REMD simulations (40 replicas between 305 and 410 , each replica 500 ns long and up to a total of ∼20 μs simulation time) to brute-force search possible Aβ−hIAPP intermediates during the cross-sequence aggregation process. For each CG-REMD replica, Aβ and hIAPP pentamers were randomly placed at different positions with a separation distance of at least 16 Å and with different initial Boltzmann-distributed atomic velocities, which allow more conformational space coverage and enhanced sampling efficiency in a rugged

free energy landscape. Figure 3 presented the time-dependent R_g distributions of Aβ−hIAPP aggregates using the acquired
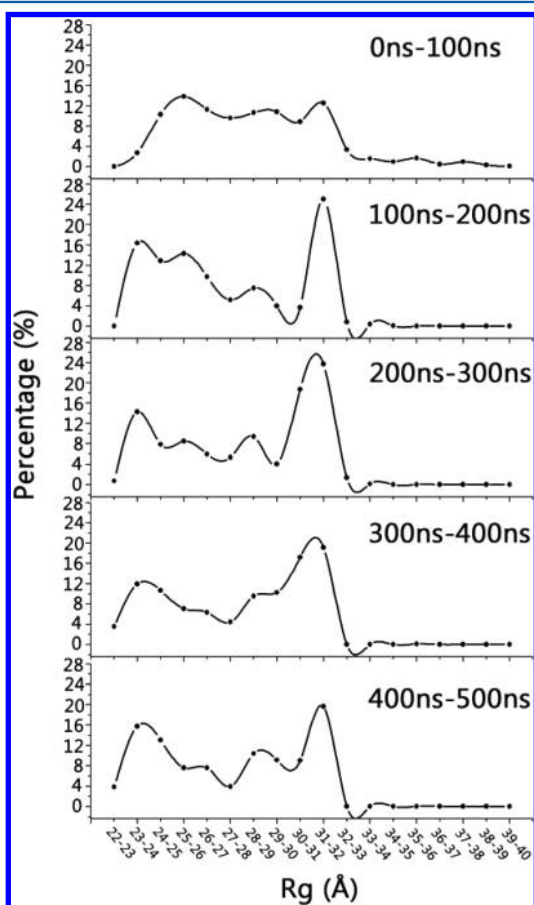
Figure 3. R_g distributions of Aβ−hIAPP aggregates at different time intervals obtained from CG-REMD simulations.

trajectories at 310 K. Overall, R_g values for hybrid Aβ−hIAPP cross-seeding species mainly spanned from 22 to 33 Å, indicating that the association of Aβ and hIAPP oligomers can lead to many intermediate complexes. In the first 100 ns, the R_g values almost evenly spanned from approximately 24 to 32 Å, with 2−3% higher populations for a few R_g values. At 100−200 ns, R_g distribution greatly shifted its size populations of Aβ−hIAPP aggregates, with one pronounced sharp peak at 30−32 Å and another broad peak near 23−26 Å. As simulations further proceeded to 200−500 ns, we found that three R_g curves at the three time intervals (200−300, 300−400, and 400−500 ns) were almost identical, where the two major R_g peaks remained almost unchanged at 23−26 and 30−32 Å. This suggests that a rough equilibrium is established after 200 ns. Thus, all analyses discussed below pertain to the last 400 ns trajectories at the temperature replica at 310 K.

To capture and characterize possible Aβ−hIAPP aggregates at many intermediate states, we used the two reaction coordinates of R_g and RMSD to construct a free energy landscape along the aggregation process of Aβ and hIAPP pentamers. It can be seen in Figure 4 that four local basins in the free energy landscape of Aβ−hIAPP complexes were identified at (R_g, RMSD) values of (22−24.5, 21−26 Å), (41−44, 28−29 Å), (69−80, 30.5−32 Å), and (60−64, 23.3−23.8 Å), respectively. Due to the complex polymorphic nature of amyloid aggregation, many basins may contain different

topologies from the two pentamers. By comparing various topologies of Aβ−hIAPP complexes, we identified the four most populated common structures from four different basins, and these four Aβ−hIAPP topologies were stabilized by different patterns of side chain interactions. Specifically, the basin (22−24.5, 21−26 Å) showed one typical double-layer topological structure, in which Aβ and hIAPP pentamers were associated together laterally by forming an interface between the N-terminal β-sheet of Aβ and C-terminal β-sheet of hIAPP. Double-layer structures of different homoamyloid peptides (e.g., Aβ, hIAPP, GNNQQNY) have been often observed by experiments and simulations.[35,58,78,79] In the basin of (60−64, 23.3−23.8 Å), the elongation mode was observed, i.e. Aβ and hIAPP were associated together along with the fibril axis in a relative register manner. Double-layer and elongation models are considered as the two most common structural motifs for facilitating amyloid formation and amyloid polymorphism. The former increases the fibril thickness, while the latter increase the fibril length. We further identified two populated association models: a tail−tail association model from the basin of (41−44, 28−29 Å) and a block association model from the basin of (69−80, 30.5−32 Å). The tail−tail association model enabled Aβ and hIAPP to interact with each other via their terminals, and two pentamers in the aggregated state showed a large orientation angle of ∼90°. Such organization and orientation only allows two pentamers to be grown into large hybrid fibrils via the elongation pathway. In the block model that differs from other three models, the turn region of Aβ pentamer was attached to the edge of hIAPP, leading to the fibril axis of the two pentamers were perpendicular to each other; in this way the elongation of hIAPP was largely blocked by Aβ attachment. Overall, four different association modes suggest the coexistence of different aggregation pathways for cross-β-sheet assemblies and reorganization between Aβ and hIAPP oligomers. Among them, double-layer and elongation association modes have a tight interface between Aβ and hIAPP oligomers, suggesting the critical nucleus or building blocks that might play an important role in cross-sequence fibrillization. The tail−tail mode with a marginally contacting interface provides additional fibrillization pathway, but with a low occurring probability. In contrast, the block mode is likely to inhibit the formation of hybrid Aβ−hIAPP fibrils.

Polymorphic Structures and Association Modes of All-Atom Aβ−hIAPP Aggregates. The CG-derived Aβ−hIAPP aggregates (Figure 4) were then converted into the corresponding all-atom structures using an in-house code, as described in the Materials and Methods section. After conversion, the resulting all-atom Aβ−hIAPP aggregates exhibited the reasonably structural consistency with the CG-based aggregates, with well-preserved interpeptide interfaces and overall β-sheet conformations. Four Aβ−hIAPP aggregates were tested to explore variations in their structural stability and association modes, with particular attention to different matches of β-sheet layers, using 60 ns all-atom MD simulations. The averaged structures (Figure 5), along with visual inspection of the trajectories, confirmed that all Aβ−hIAPP aggregates retained the same interfacial residue contacts and association modes as those in CG presentations. Some minor structural adjustments occurred at the interfaces, but no dissociation events and large structural disturbance were observed for these all-atom aggregates. We further analyzed the structural characteristics of four hybrid Aβ−hIAPP aggregates using the data from RMSD, RMSF, and secondary structure content
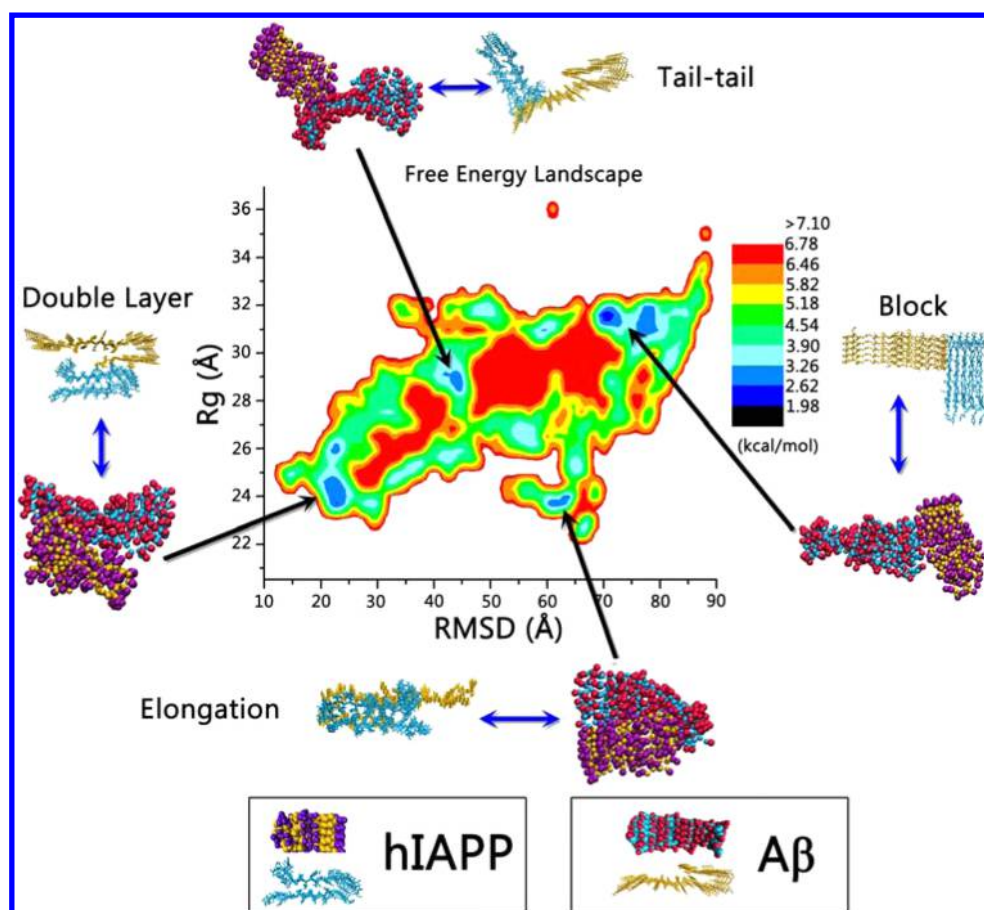
Figure 4. CG-based free energy landscape along Aβ and hIAPP aggregation process as a function of two reaction coordinations of R_g and RMSD. The all-atom Aβ−hIAPP structures were obtained from the corresponding CG Aβ−hIAPP structures at different local energy minima.
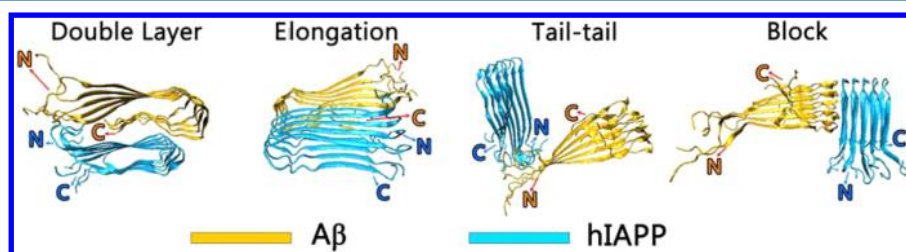
Figure 5. All-atom Aβ−hIAPP structures with double-layer, elongation, tail−tail, and block association modes, averaged from the last 10 ns MD trajectories. N and C refer to N- and C-termini, respectively.
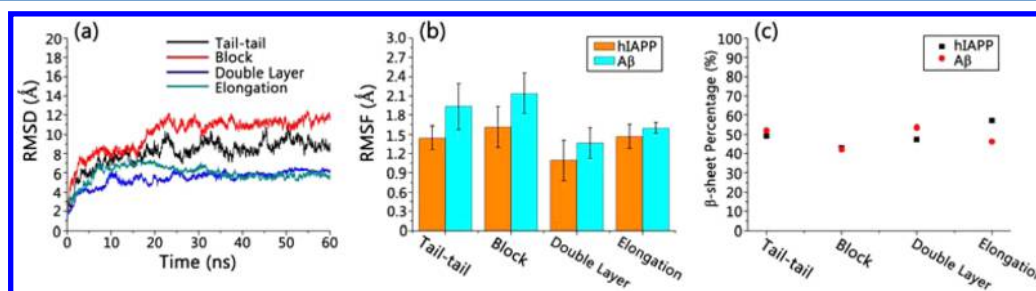

Figure 6. Structural characterization of all-atom Aβ−hIAPP heteroassemblies using (a) RMSD, (b) RMSF, and (c) β-sheet percentages.

(Figure 6). For all Aβ−hIAPP heteroassemblies, the RMSD profiles achieved the relatively stable plateau after 30 ns, indicating that the modeled heteroassemblies reached the local structural equilibrium during 60 ns MD simulations. Upon association, both Aβ and hIAPP were able to retain their overall U-shaped conformations and dominant β-sheet contents. Specifically, in all cases hIAPP and Aβ pentamers had comparable β-sheet percentages of 42.8−56.9% and 42.2−53.5%, respectively. RMSF values showed that Aβ pentamers had slightly larger structural fluctuations than hIAPP pentamers
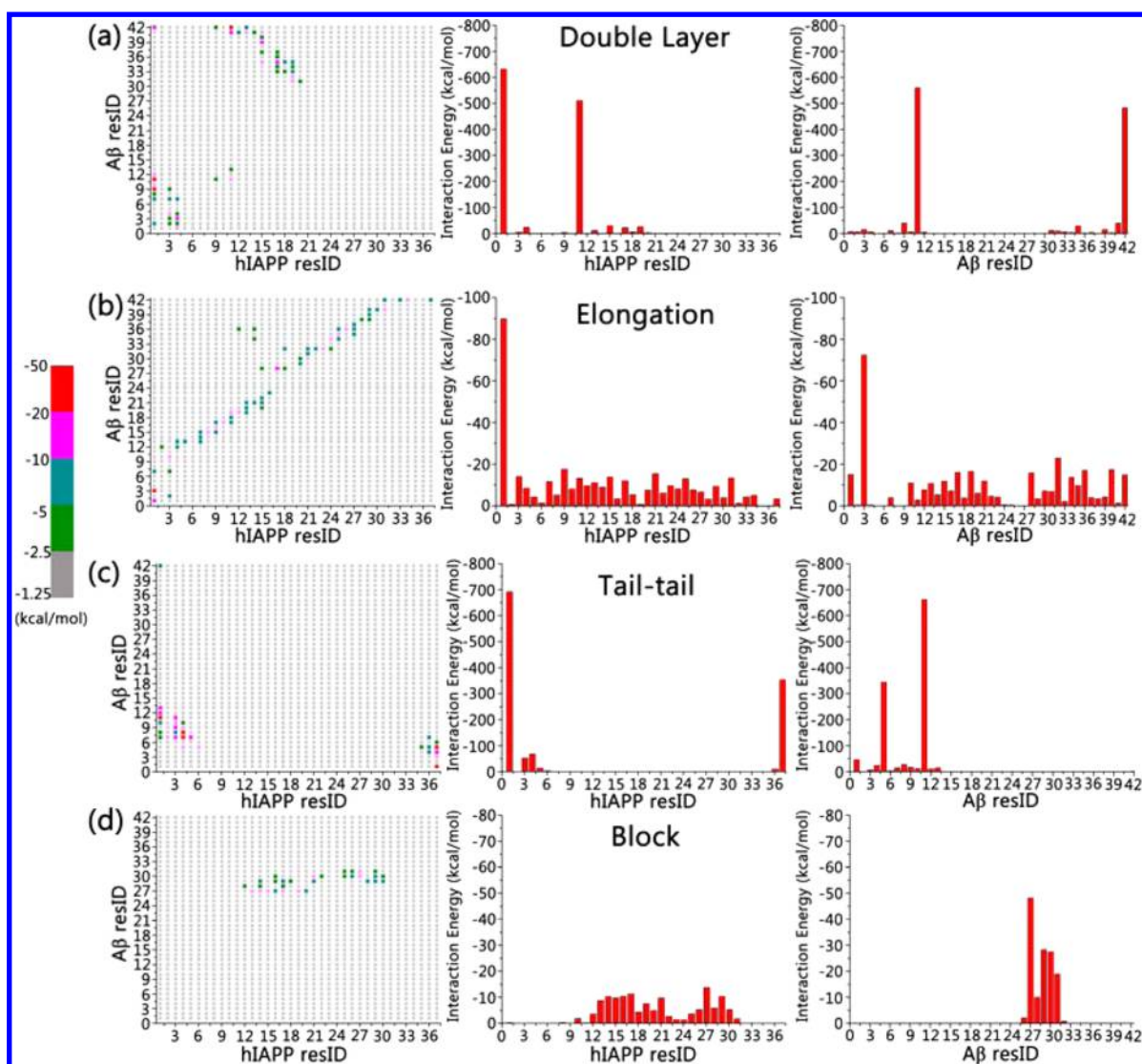
Figure 7. Intermolecular interactions between all residues of hIAPP and all residues of Aβ, between all residues of hIAPP and Aβ, and between all residues of Aβ and hIAPP for (a) double-layer, (b) elongation, (c) tail−tail, and (d) block Aβ−hIAPP heteroassemblies.

(RMSF values). Visual inspection of MD trajectories indicated that the relatively higher fluctuations of Aβ pentamers mainly came from the N-terminal regions (residue 1−16). Among the four Aβ−hIAPP assemblies, double-layer model was identified as the most stable assembly as supported by small RMSD, RMSF, and R_g values.

To better quantify association forces and identify interaction residues at different interfaces, Figure 7 shows intermolecular interactions between all residues of hIAPP and all residues of Aβ, between all residues of hIAPP and Aβ, and between all residues of Aβ and hIAPP. For the double-layer model, the interface mainly consisted of two strong interacting regions: one between C-terminal-β-sheet of Aβ (residue 31−42) and N-terminal-β-sheet of hIAPP (residue 9−20) and the other between C-terminal residues of Aβ (residue 1−12) and C-terminal turn residues of hIAPP (residue 1−4). The Aβ−hIAPP binding also made the involved residues more stable, as indicated by the relatively low RMSF values in Figure 8a. The two interaction regions provided strong interactions (−1237.2 kcal/mol, Figure 9a) and large contacts (1713.7 Å^2) to associate Aβ and hIAPP together. In Figure 9a, decomposition of a total of interaction energy between Aβ and hIAPP revealed that

electrostatic interactions (92.3%) significantly contributed to the total Aβ−hIAPP interactions. At the double-layer interface, ∼29.6 hydrogen bonds, ∼33.1 hydrophobic contacts, and ∼4 salt bridges were simultaneously observed, indicating that the double-layer interface is synergistically stabilized by various intermolecular forces. The residue-based interaction energies, along with the visual inspection of MD trajectories, clearly revealed an important role of interfacial salt bridges of $R_{hiapp}{}^{11}$−$A_{Aβ}{}^{42}$ and $K_{hiapp}{}^{1}$−$E_{Aβ}{}^{11}$ in stabilizing forces (Figure 7a), interpreting high contribution of electrostatic interactions to the Aβ−hIAPP double-layer assembly (Figure 9a).

For the elongation model, Aβ and hIAPP pentamers were associated together via stable end-to-end interactions. The elongation assembly presented an almost seamless interface by aligning two similar U-bend conformations along the fibril direction (Figure 5), which is very similar to addition of homopeptides to the edges of existing homoamyloid assemblies. The elongation assembly can still well preserve its structural integrity and present high structural stability throughout the simulations, as confirmed by its small and steady RMSD, RMSF, and R_g values (Figures 6 and 8b). The residue−residue interaction map clearly identified a series of
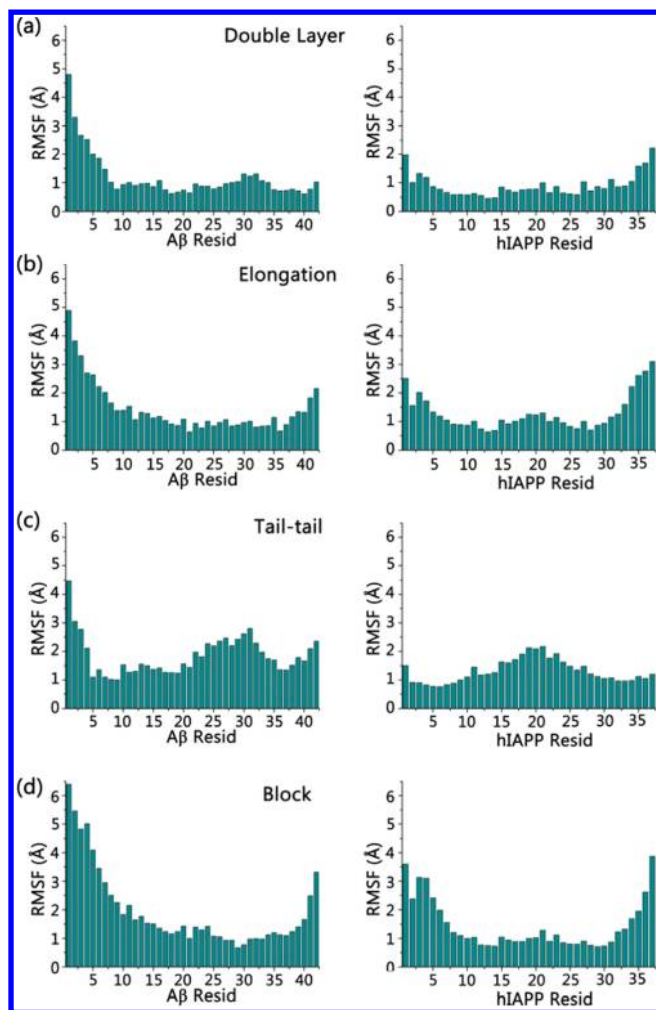
Figure 8. Residue-based RMSF values for Aβ–hIAPP assemblies of (a) double layer, (b) elongation, (c) tail–tail, and (d) block models.

moderate interacting residues along diagonal axis, indicating that almost all β-sheet strand residues (residue 12−42 for Aβ and residue 3−30 for hIAPP) contribute to interfacial interactions in the range of −5 to −20 kcal/mol (Figure 7b). These moderate interacting residues also formed ∼17.1 backbone hydrogen bonds, ∼10.2 hydrophobic side-chain contacts, and 2 salt bridges between K_{hiapp}^{1} and $E_{Aβ}^{3}$. These different interfacial contacts resemble the structural basis and association pattern of homoamyloid assemblies.

The "tail−tail" model showed Aβ and hIAPP to be associated together via their N/C-terminal regions, forming a "V" shape morphology. This hybrid assembly (RMSD = 9.2 Å and RMSF = 1.4−1.9 Å) showed slightly higher structural flexibility than both double-layer and elongation assemblies (Figure 6a and b). We observed that hIAPP and Aβ pentamers continuously adjusted their local positions and orientations to optimize interfacial interaction, but surprisingly, they did not disassociate with each other within 60 ns MD simulations, only with a slighter higher residue fluctuation compared to double layer and elongation models (Figure 8c). This is probably due to highly favorable interactions (−1161.9 kcal/mol) between hIAPP and Aβ pentamers. The residue-based interaction analysis showed that the tail−tail assembly had a total of (i) ∼6 salt bridges formed between K_{hiapp}^{1}−$E_{Aβ}^{11}$ and Y_{hiapp}^{37}−$R_{Aβ}^{5}$ and (ii) ∼38.6 hydrogen bonds between polar residues at both N/C-terminal regions. These interactions undoubtedly stabilized the assembly and electrostatic interactions contributed to 96% of total Aβ−hIAPP interaction for association.

In the block model, the turn region (residues 26−32) of Aβ was associated with the edge region (residues 10−31) of hIAPP in a perpendicular orientation. This association mode led to the relatively larger overall structural flexibility (RMSD = 11.5 Å and RMSF = 1.8 Å) and residue-based fluctuation (Figure 8d). But structural flexibility was only limited to the two terminal regions that are highly exposed to solvent and did not affect the Aβ−hIAPP association at the interface. The interaction energy was the smallest one (−154.8 kcal/mol) among four models, where VDW and electrostatics interactions had comparable contributions. Consistently, the block assembly only involved ∼6.7 hydrogen bonds and ∼6.1 hydrophobic contacts at the interface. In sharp contrast to other three assemblies, in the block assembly Aβ peptides will block the growing ends of hIAPP and interfere with their elongation into amyloid fibrils. Overall, different hybrid Aβ−hIAPP assemblies with different interfaces reflect complex heteroassembly pathways driven by different interfacial interactions.

Structural Populations of Polymorphic Aβ−hIAPP Assemblies. To better rationale the structural preference of four different Aβ−hIAPP aggregates, using all four models and 2000 conformations (500 conformations per each model) extracted from the last 10 ns MD trajectories, we estimate the relative population for each model using an in-house MC program and the GBMV implicit-solvent method. The GBMV implicit-solvent method allows to compute the relative conformational energies of all constructed models, while the
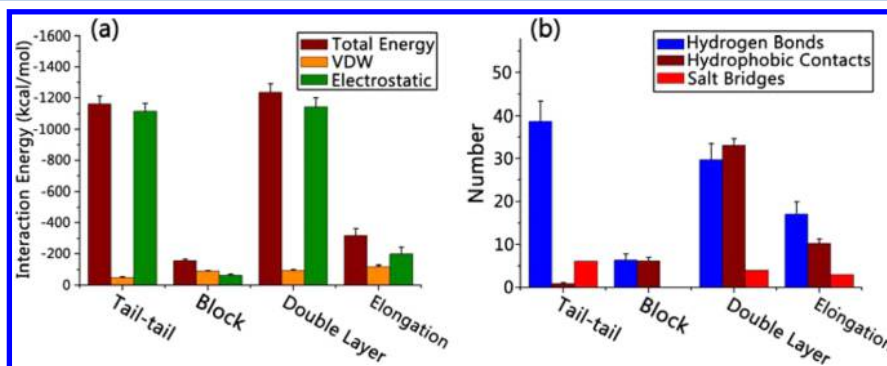

Figure 9. (a) Nonbonded interaction energy and its decompositions and (b) nonbonded interfacial contacts between Aβ and hIAPP for four all-atom Aβ−hIAPP heteroassemblies.

MC simulation allows to estimate the relative populations for each model, as we previously applied for other amyloids.[72] The combination of GBMV and MC methods will provide polymorphic and thermodynamic properties of the Aβ–hIAPP cross-seeding aggregates.

Figure 10 summarizes the relative structural populations for the four different Aβ–hIAPP models. Overall, the structural
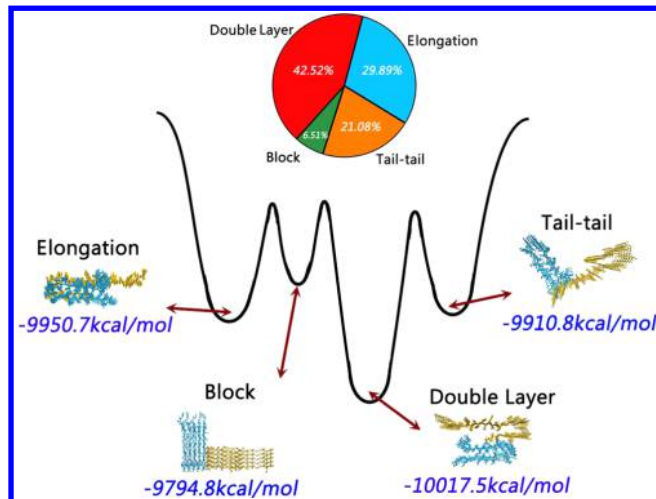
Figure 10. Structural populations and overall conformational energies for four all-atom Aβ–hIAPP heteroassemblies.

populations of the four models range from 6.51% to 42.52%, highlighting the polymorphic nature of Aβ–hIAPP cross-seeding assemblies. Among them, double-layer model of Aβ–hIAPP has the highest structural population of 42.5% and the lowest conformational energy of −10 017.5 kcal/mol. The double-layer models have been proposed for many homo-amyloid polypeptides including Aβ, hIAPP, and GNNQQNY.[78−82] Mass-per-length data show that the double-layer models are the most populated morphology for Aβ and hIAPP fibrils.[54,83] The double-layer models provide different β-sheet arrangement possibilities for amyloid oligomers and fibrils to be associated laterally. The second populated cross-seeding assembly was the elongation model (29.9%). The peptide elongation along the fibril axis is one of the most common aggregation pathways for all homoamyloid peptides. In this case, it is conceivable that Aβ and hIAPP with similar structures and compatible fitting interfaces could interact with these β-pleated sheet domains via a similar fibril formation mechanism. Both amyloid seeds from hIAPP and Aβ peptides could serve as the interacting precursors to mutually promote the amyloid elongation. Consistently, a number of studies have reported that amyloids from different species or with different sequences can overcome cross-seeding barriers to form cross-seeding aggregates and fibrils via the elongation pathway if they have close structural similarity, including tau-k18 and tau-k19,[84−87] Aβ and tau,[29] and hIAPP and rIAPP.[25] Meanwhile, it is interesting to note that the tail−tail model also had a relatively higher population of 21.1%. This suggests another possible aggregation pathway: hIAPP and Aβ peptides could employ their terminal residues as the cross-seeding "tentacles" to hold β-sheets for fiber growth. By contrast, the block model only presented the lowest population of 6.5%, probably due to its high enthalpy state induced by the smaller interaction energies. However, we should not neglect this block model and other possible structural models that may have

similar stabilities and relatively smaller populations that we did not examine in this study. These ensembles of structures with relatively smaller populations may be due to different peptide associations and even small structural fluctuation in a specific domain. For example, recently Miller and co-workers[81] have found that a subtle change of single residue orientation at the turn region of hIAPP can dramatically change fibril structures and assembly pathways of hIAPP.

It is also interesting to compare the gain or loss of conformational energies between two unbound Aβ and hIAPP pentamers and the four associated Aβ–hIAPP assemblies. The conformational energies of free unbound Aβ and hIAPP pentamers were −5461.8 and −4371.2 kcal/mol, respectively. The overall conformational energies of the four Aβ–hIAPP assemblies were in an increase order of double-layer (−10017.5 kcal/mol) < elongation (−9950.7 kcal/mol) < tail−tail (−9910.8 kcal/mol) < block (−9794.8 kcal/mol), consistent with the order of the structural population distributions of the four hybrid assemblies. It can be seen clearly that upon association, the double layer, elongation, and tail−tail assemblies lose the energy as compared to the summation of conformational energies of the two unbound Aβ and hIAPP pentamers, indicating that these associations are energy favorable process. Instead, the block assembly requires additional energy to assist two unbound pentamers to be associated together, which is energy unfavorable process. We should note that the cross-sequence interactions between Aβ and hIAPP do not necessarily imply the acceleration of the aggregation process of Aβ and hIAPP. Instead, depending on association efficiency between Aβ and hIAPP and relative structural populations of different Aβ and hIAPP aggregates, the aggregation process could be either delayed or accelerated at different aggregation stages, leading to inhibition or promotion effects. The double layer, elongation, and tail−tail models are good templates for the acceleration of fiber growth, while the block model may cause the inhibition effects on amyloid formation.

■ CONCLUSIONS

Understanding the cross-sequence aggregation mechanisms between different Aβ and hIAPP peptides is critical for revealing a potential pathological link between AD and T2D. In this work, we systematically modeled and simulated the aggregation process of Aβ and hIAPP peptides and probed different association modes between Aβ and hIAPP on Aβ–hIAPP hybrid structures, conformational dynamics, and structural populations using combined coarse-grain and all-atom MD simulations. The coarse-grained MD simulations allow to coarsely and quickly determine hybrid Aβ–hIAPP aggregates and their corresponding association modes, while the all-atom MD simulations enable to examine the atomic details of Aβ–hIAPP interaction modes and the structural dynamics of Aβ–hIAPP aggregates. Collective simulation results confirmed that Aβ and hIAPP can indeed associate with each other to form stable hybrid aggregates via different β-sheet arrangements. Four Aβ–hIAPP aggregates of double-layer, elongation, tail−tail, and block were determined at the lowest energy states. The interfaces involving in these hybrid aggregates were synergistically stabilized by hydrogen bonds, hydrophobic contacts, and salt bridges, but these interfacial interactions contribute differently to different Aβ–hIAPP aggregates and to different association modes. These hybrid Aβ–hIAPP aggregates displayed different interacting interfaces

and were driven by different interfacial interactions, demonstrating that the coexistence of polymorphic amyloid cross-seeding species through different aggregation pathways. Among four Aβ−hIAPP models tested, the double-layer and elongation models were demonstrated to be prominent with respect to other two assemblies (i.e., block and tail−tail), as supported by their higher structural population, the lower conformational energy and the better structural stability. This clearly indicates that the lateral association and axial elongation are the most likely cross-seeding aggregation pathways compared to other scenarios. Instead, the block model might exert certain inhibition effect on fiber propagation. We should note that the proposed computational models do not rule out other potential hybrid intermediates or assemblies, whose structures and populations are currently difficult to be detected, but always need to be validated by future experiments. The cross-sequence interactions between Aβ and hIAPP, as demonstrated by our simulations, could be helpful for a better fundamental understanding of a molecular link between AD and T2D diseases.

■ AUTHOR INFORMATION

Corresponding Author

*E-mail: zhengj@uakron.edu.

Notes

The authors declare no competing financial interest.

■ ACKNOWLEDGMENTS

■ REFERENCES

(1) Cleary, J. P.; Walsh, D. M.; Hofmeister, J. J.; Shankar, G. M.; Kuskowski, M. A.; Selkoe, D. J.; Ashe, K. H. Natural Oligomers of the Amyloid-β Protein Specifically Disrupt Cognitive Function. *Nat. Neurosci.* **2005**, *8*, 79−84.

(2) Irvine, G. B.; El-Agnaf, O. M.; Shankar, G. M.; Walsh, D. M. Protein Aggregation in the Brain: the Molecular Basis for Alzheimer's and Parkinson's Diseases. *Mol. Med.* **2008**, *14*, 451−464.

(3) Haataja, L.; Gurlo, T.; Huang, C. J.; Butler, P. C. Islet Amyloid in Type 2 Diabetes, and the Toxic Oligomer Hypothesis. *Endocr. Rev.* **2008**, *29*, 303−316.

(4) Epstein, F. H.; Ahren, B.; Lips, C. J.; Hoppener, J. W. Islet Amyloid and Type 2 Diabetes Mellitus. *N. Engl. J. Med.* **2000**, *343*, 411−419.

(5) Brender, J. R.; Salamekh, S.; Ramamoorthy, A. Membrane Disruption and Early Events in the Aggregation of the Diabetes Related Peptide IAPP from a Molecular Perspective. *Acc. Chem. Res.* **2012**, *45*, 454−462.

(6) Truant, R.; Atwal, R. S.; Desmond, C.; Munsie, L.; Tran, T. Huntington's Disease: Revisiting the Aggregation Hypothesis in Polyglutamine Neurodegenerative Diseases. *FEBS J.* **2008**, *275*, 4252−4262.

(7) Goedert, M.; Alpha-Synuclein. and Neurodegenerative Diseases. *Nat. Rev. Neurosci.* **2001**, *2*, 492−501.

(8) Zhang, M. Z.; Zhao, J.; Zheng, J. Molecular Understanding of a Potential Functional Link between Antimicrobial and Amyloid Peptides. *Soft Matter* **2014**, *10*, 7425−7451.

(9) Wang, Q. M.; Liang, G. Z.; Zhang, M. Z.; Zhao, J.; Patel, K.; Yu, X.; Zhao, C.; Ding, B. R.; Zhang, G.; Zhou, F. M.; Zheng, J. De Novo Design of Self-Assembled Hexapeptides as β-Amyloid (Aβ) Peptide Inhibitors. *ACS Chem. Neurosci.* **2014**, *5*, 972−981.

(10) Stefani, M. Structural Features and Cytotoxicity of Amyloid Oligomers: Implications in Alzheimer's Disease and Other Diseases with Amyloid Deposits. *Prog. Neurobiol.* **2012**, *99*, 226−245.

(11) Tofoleanu, F.; Brooks, B. R.; Buchete, N. V. Modulation of Alzheimer's Aβ Protofilament-Membrane Interactions by Lipid Headgroups. *ACS Chem. Neurosci.* **2015**, *6*, 446−455.

(12) Nasica-Labouze, J.; Nguyen, P. H.; Sterpone, F.; Berthoumieu, O.; Buchete, N.-V.; Coté, S.; De Simone, A.; Doig, A. J.; Faller, P.; Garcia, A.; Laio, A.; Li, M. S.; Melchionna, S.; Mousseau, N.; Mu, Y.; Paravastu, A.; Pasquali, S.; Rosenman, D. J.; Strodel, B.; Tarus, B.; Viles, J. H.; Zhang, T.; Wang, C.; Derreumaux, P. Amyloid-β Protein and Alzheimer's Disease: When Computer Simulations Complement Experimental Studies. *Chem. Rev.* **2015**, *115*, 3518−3563.

(13) Cao, P.; Marek, P.; Noor, H.; Patsalo, V.; Tu, L. H.; Wang, H.; Abedini, A.; Raleigh, D. P. Islet Amyloid: From Fundamental Biophysics to Mechanisms of Cytotoxicity. *FEBS Lett.* **2013**, *587*, 1106−1118.

(14) Miller, Y.; Ma, B. Y.; Nussinov, R. Alzheimer Aβ Amyloid Annular Fibrils: Insight into Polymorphism. *Biophys. J.* **2011**, *100*, 531−531.

(15) Srivastava, A.; Balaji, P. V. Size, Orientation and Organization of Oligomers that Nucleate Amyloid Fibrils: Clues from MD Simulations of Pre-Formed Aggregates. *Biochim. Biophys. Acta, Proteins Proteomics* **2012**, *1824*, 963−973.

(16) Qi, R.; Luo, Y.; Ma, B.; Nussinov, R.; Wei, G. Conformational Distribution and α-Helix to β-Sheet Transition of Human Amylin Fragment Dimer. *Biomacromolecules* **2014**, *15*, 122−131.

(17) Vitrenko, Y. A.; Gracheva, E. O.; Richmond, J. E.; Liebman, S. W. Visualization of Aggregation of the Rnq1 Prion Domain and Cross-Seeding Interactions with Sup35NM. *J. Biol. Chem.* **2007**, *282*, 1779−1787.

(18) Yan, J.; Fu, X.; Ge, F.; Zhang, B.; Yao, J.; Zhang, H.; Qian, J.; Tomozawa, H.; Naiki, H.; Sawashita, J.; Mori, M.; Higuchi, K. Cross-Seeding and Cross-Competition in Mouse Apolipoprotein A-II Amyloid Fibrils and Protein A Amyloid Fibrils. *Am. J. Pathol.* **2007**, *171*, 172−180.

(19) Ma, B.; Nussinov, R. Selective Molecular Recognition in Amyloid Growth and Transmission and Cross-Species Barriers. *J. Mol. Biol.* **2012**, *421*, 172−184.

(20) Guo, C.; Cote, S.; Mousseau, N.; Wei, G. Distinct Helix Propensities and Membrane Interactions of Human and Rat IAPP1−19 Monomers in Anionic Lipid Bilayers. *J. Phys. Chem. B* **2015**, *119*, 3366−76.

(21) Ramamoorthy, A. Insights into Protein Misfolding and Amyloidogenesis. *Phys. Chem. Chem. Phys.* **2013**, *15*, 8867−8867.

(22) O'Nuallain, B.; Williams, A. D.; Westermark, P.; Wetzel, R. Seeding Specificity in Amyloid Growth Induced by Heterologous Fibrils. *J. Biol. Chem.* **2004**, *279*, 17490−17499.

(23) Hu, R. D.; Zhang, M. Z.; Patel, K.; Wang, Q. M.; Chang, Y.; Gong, X.; Zhang, G.; Zheng, J. Cross-Sequence Interactions between Human and Rat Islet Amyloid Polypeptides. *Langmuir* **2014**, *30*, 5193−5201.

(24) Andreetto, E.; Yan, L. M.; Caporale, A.; Kapurniotu, A. Dissecting the Role of Single Regions of an IAPP Mimic and IAPP in Inhibition of Aβ40 Amyloid Formation and Cytotoxicity. *ChemBioChem* **2011**, *12*, 1313−1322.

(25) Zhang, M. Z.; Hu, R. D.; Liang, G. Z.; Chang, Y.; Sun, Y.; Peng, Z. M.; Zheng, J. Structural and Energetic Insight into the Cross-Seeding Amyloid Assemblies of Human IAPP and Rat IAPP. *J. Phys. Chem. B* **2014**, *118*, 7026−7036.

(26) Morales, R.; Estrada, L. D.; Diaz-Espinoza, R.; Morales-Scheihing, D.; Jara, M. C.; Castilla, J.; Soto, C. Molecular Cross Talk between Misfolded Proteins in Animal Models of Alzheimer's and Prion Diseases. *J. Neurosci.* **2010**, *30*, 4528−4535.

(27) Seeliger, J.; Evers, F.; Jeworrek, C.; Kapoor, S.; Weise, K.; Andreetto, E.; Tolan, M.; Kapurniotu, A.; Winter, R. Cross-Amyloid Interaction of Aβ and IAPP at Lipid Membranes. *Angew. Chem., Int. Ed.* **2012**, *51*, 679−683.

(28) Ono, K.; Takahashi, R.; Ikeda, T.; Yamada, M. Cross-Seeding Effects of Amyloid β-Protein and α-Synuclein. *J. Neurochem.* **2012**, *122*, 883−890.

(29) Miller, Y.; Ma, B.; Nussinov, R. Synergistic Interactions between Repeats in Tau Protein and Aβ Amyloids may be Responsible for Accelerated Aggregation via Polymorphic States. *Biochemistry* **2011**, *50*, 5172−5181.

(30) Guo, J. P.; Arai, T.; Miklossy, J.; McGeer, P. L. Aβ and Tau Form Soluble Complexes that may Promote Self Aggregation of Both into the Insoluble Forms Observed in Alzheimer's Disease. *Proc. Natl. Acad. Sci. U. S. A.* **2006**, *103*, 1953−1958.

(31) Berhanu, W. M.; Yasar, F.; Hansmann, U. H. In Silico Cross Seeding of Aβ and Amylin Fibril-Like Oligomers. *ACS Chem. Neurosci.* **2013**, *4*, 1488−1500.

(32) Bernhardt, N. A.; Berhanu, W. M.; Hansmann, U. H. Mutations and Seeding of Amylin Fibril-Like Oligomers. *J. Phys. Chem. B* **2013**, *117*, 16076−16085.

(33) Berhanu, W. M.; Hansmann, U. H. Inter-Species Cross-Seeding: Stability and Assembly of Rat-Human Amylin Aggregates. *PLoS One* **2014**, *9*, e97051.

(34) Wu, C.; Shea, J. E. Structural Similarities and Differences between Amyloidogenic and Non-Amyloidogenic Islet Amyloid Polypeptide (IAPP) Sequences and Implications for the Dual Physiological and Pathological Activities of these Peptides. *PLoS Comput. Biol.* **2013**, *9*, e1003211.

(35) Wu, C.; Bowers, M. T.; Shea, J. E. Molecular Structures of Quiescently Grown and Brain-Derived Polymorphic Fibrils of the Alzheimer Amyloid Aβ9−40 Peptide: a Comparison to Agitated Fibrils. *PLoS Comput. Biol.* **2010**, *6*, e1000693.

(36) Yamamoto, N.; Matsuzaki, K.; Yanagisawa, K. Cross-Seeding of Wild-Type and Hereditary Variant-Type Amyloid β-Proteins in the Presence of Gangliosides. *J. Neurochem.* **2005**, *95*, 1167−1176.

(37) Cereda, E.; Barichella, M.; Pedrolli, C.; Klersy, C.; Cassani, E.; Caccialanza, R.; Pezzoli, G. Diabetes and Risk of Parkinson's Disease: a Systematic Review and Meta-Analysis. *Diabetes Care* **2011**, *34*, 2614−2623.

(38) Janson, J.; Laedtke, T.; Parisi, J. E.; O'Brien, P.; Petersen, R. C.; Butler, P. C. Increased Risk of Type 2 Diabetes in Alzheimer Disease. *Diabetes* **2004**, *53*, 474−481.

(39) Nicolls, M. R. The Clinical and Biological Relationship between Type II Diabetes Mellitus and Alzheimer's Disease. *Curr. Alzheimer Res.* **2004**, *1*, 47−54.

(40) Ghiso, J. A.; Holton, J.; Miravalle, L.; Calero, M.; Lashley, T.; Vidal, R.; Houlden, H.; Wood, N.; Neubert, T. A.; Rostagno, A.; Plant, G.; Revesz, T.; Frangione, B. Systemic Amyloid Deposits in Familial British Dementia. *J. Biol. Chem.* **2001**, *276*, 43909−43914.

(41) Andreetto, E.; Yan, L. M.; Tatarek-Nossol, M.; Velkova, A.; Frank, R.; Kapurniotu, A. Identification of Hot Regions of the Aβ-IAPP Interaction Interface as High-Affinity Binding Sites in both Cross- and Self-Association. *Angew. Chem., Int. Ed.* **2010**, *49*, 3081−3085.

(42) Reitz, C. Alzheimer's Disease and the Amyloid Cascade Hypothesis: a Critical Review. *Int. J. Alzheimer's Dis.* **2012**, *2012*, 369808.

(43) Kapurniotu, A. Amyloidogenicity and Cytotoxicity of Islet Amyloid Polypeptide. *Biopolymers* **2001**, *60*, 438−459.

(44) May, P. C.; Boggs, L. N.; Fuson, K. S. Neurotoxicity of Human Amylin in Rat Primary Hippocampal Cultures: Similarity to Alzheimer's Disease Amyloid-β Neurotoxicity. *J. Neurochem.* **1993**, *61*, 2330−2333.

(45) Middleton, C. T.; Marek, P.; Cao, P.; Chiu, C. C.; Singh, S.; Woys, A. M.; de Pablo, J. J.; Raleigh, D. P.; Zanni, M. T. Two-Dimensional Infrared Spectroscopy Reveals the Complex Behaviour of an Amyloid Fibril Inhibitor. *Nat. Chem.* **2012**, *4*, 355−360.

(46) Butterfield, S. M.; Lashuel, H. A. Amyloidogenic Protein-Membrane Interactions: Mechanistic Insight from Model Systems. *Angew. Chem., Int. Ed.* **2010**, *49*, 5628−5654.

(47) Stefani, M. Biochemical and Biophysical Features of Both Oligomer/Fibril and Cell Membrane in Amyloid Cytotoxicity. *FEBS J.* **2010**, *277*, 4602−4613.

(48) Weise, K.; Radovan, D.; Gohlke, A.; Opitz, N.; Winter, R. Interaction of hIAPP with Model Raft Membranes and Pancreatic β-Cells: Cytotoxicity of hIAPP Oligomers. *ChemBioChem* **2010**, *11*, 1280−1290.

(49) Williams, T. L.; Serpell, L. C. Membrane and Surface Interactions of Alzheimer's Aβ Peptide–Insights into the Mechanism of Cytotoxicity. *FEBS J.* **2011**, *278*, 3905−3917.

(50) Beaumont, K.; Kenney, M. A.; Young, A. A.; Rink, T. J. High Affinity Amylin Binding Sites in Rat Brain. *Mol. Pharmacol.* **1993**, *44*, 493−497.

(51) Mulder, H.; Leckstrom, A.; Uddman, R.; Ekblad, E.; Westermark, P.; Sundler, F. Islet Amyloid Polypeptide (Amylin) Is Expressed in Sensory Neurons. *J. Neurosci.* **1995**, *15*, 7625−7632.

(52) Paxinos, G.; Chai, S. Y.; Christopoulos, G.; Huang, X. F.; Toga, A. W.; Wang, H. Q.; Sexton, P. M. In Vitro Autoradiographic Localization of Calcitonin and Amylin Binding Sites in Monkey Brain. *J. Chem. Neuroanat.* **2004**, *27*, 217−236.

(53) Miklossy, J.; Qing, H.; Radenovic, A.; Kis, A.; Vileno, B.; Laszlo, F.; Miller, L.; Martins, R. N.; Waeber, G.; Mooser, V.; Bosman, F.; Khalili, K.; Darbinian, N.; McGeer, P. L. Beta Amyloid and Hyperphosphorylated Tau Deposits in the Pancreas in Type 2 Diabetes. *Neurobiol. Aging* **2010**, *31*, 1503−1515.

(54) Luca, S.; Yau, W. M.; Leapman, R.; Tycko, R. Peptide Conformation and Supramolecular Organization in Amylin Fibrils: Constraints from Solid-State NMR. *Biochemistry* **2007**, *46*, 13505−13522.

(55) Luhrs, T.; Ritter, C.; Adrian, M.; Riek-Loher, D.; Bohrmann, B.; Dobeli, H.; Schubert, D.; Riek, R. 3D Structure of Alzheimer's Amyloid-β(1−42) Fibrils. *Proc. Natl. Acad. Sci. U. S. A.* **2005**, *102*, 17342−17347.

(56) Xiao, Y.; Ma, B.; McElheny, D.; Parthasarathy, S.; Long, F.; Hoshi, M.; Nussinov, R.; Ishii, Y. Aβ(1−42) Fibril Structure Illuminates Self-Recognition and Replication of Amyloid in Alzheimer's Disease. *Nat. Struct. Mol. Biol.* **2015**, *22*, 499−505.

(57) Ahmed, M.; Davis, J.; Aucoin, D.; Sato, T.; Ahuja, S.; Aimoto, S.; Elliott, J. I.; Van Nostrand, W. E.; Smith, S. O. Structural Conversion of Neurotoxic Amyloid-β(1−42) Oligomers to Fibrils. *Nat. Struct. Mol. Biol.* **2010**, *17*, 561−567.

(58) Petkova, A. T.; Yau, W. M.; Tycko, R. Experimental Constraints on Quaternary Structure in Alzheimer's β-Amyloid Fibrils. *Biochemistry* **2006**, *45*, 498−512.

(59) Paravastu, A. K.; Leapman, R. D.; Yau, W. M.; Tycko, R. Molecular Structural Basis for Polymorphism in Alzheimer's β-Amyloid Fibrils. *Proc. Natl. Acad. Sci. U. S. A.* **2008**, *105*, 18349−18354.

(60) Miller, Y.; Ma, B.; Tsai, C.-J.; Nussinov, R. Hollow Core of Alzheimer's Aβ42 Amyloid Observed by CryoEM is Relevant at Physiological pH. *Proc. Natl. Acad. Sci. U. S. A.* **2010**, *107*, 14128−14133.

(61) Liang, G.; Zhao, J.; Yu, X.; Zheng, J. Comparative Molecular Dynamics Study of Human Islet Amyloid Polypeptide (IAPP) and Rat IAPP Oligomers. *Biochemistry* **2013**, *52*, 1089−1100.

(62) Alred, E. J.; Scheele, E. G.; Berhanu, W. M.; Hansmann, U. H. Stability of Lowa Mutant and Wild Type Aβ-Peptide Aggregates. *J. Chem. Phys.* **2014**, *141*, 175101.

(63) Bitan, G.; Kirkitadze, M. D.; Lomakin, A.; Vollers, S. S.; Benedek, G. B.; Teplow, D. B. Amyloid beta -protein (Abeta) assembly: Aβ 40 and Aβ 42 Oligomerize through Distinct Pathways. *Proc. Natl. Acad. Sci. U. S. A.* **2003**, *100*, 330−335.

(64) Urbanc, B.; Cruz, L.; Yun, S.; Buldyrev, S. V.; Bitan, G.; Teplow, D. B.; Stanley, H. E. In Silico Study of Amyloid β-Protein Folding and Oligomerization. *Proc. Natl. Acad. Sci. U. S. A.* **2004**, *101*, 17345−17350.

(65) Miller, Y.; Ma, B.; Nussinov, R. Polymorphism in Alzheimer Aβ Amyloid Organization Reflects Conformational Selection in a Rugged Energy Landscape. *Chem. Rev.* **2010**, *110*, 4820−4838.

(66) Ono, K.; Condron, M. M.; Teplow, D. B. Structure Neurotoxicity Relationships of Amyloid β-Protein Oligomers. *Proc. Natl. Acad. Sci. U. S. A.* **2009**, *106*, 14745−14750.

(67) Periole, X.; Cavalli, M.; Marrink, S. J.; Ceruso, M. A. Combining an Elastic Network With a Coarse-Grained Molecular Force Field: Structure, Dynamics, and Intermolecular Recognition. *J. Chem. Theory Comput.* **2009**, *5*, 2531−2543.

(68) Brocos, P.; Mendoza-Espinosa, P.; Castillo, R.; Mas-Oliva, J.; Pineiro, A. Multiscale Molecular Dynamics Simulations of Micelles: Coarse-Grain for Self-Assembly and Atomic Resolution for Finer Details. *Soft Matter* **2012**, *8*, 9005−9014.

(69) Van der Spoel, D.; Lindahl, E.; Hess, B.; Groenhof, G.; Mark, A. E.; Berendsen, H. J. C. GROMACS: Fast, Flexible, and Free. *J. Comput. Chem.* **2005**, *26*, 1701−1718.

(70) Buck, M.; Bouguet-Bonnet, S.; Pastor, R. W.; MacKerell, A. D. Importance of the CMAP Correction to the CHARMM22 Protein Force Field: Dynamics of Hen Lysozyme. *Biophys. J.* **2006**, *90*, L36− L38.

(71) Chebaro, Y.; Dong, X.; Laghaei, R.; Derreumaux, P.; Mousseau, N. Replica Exchange Molecular Dynamics Simulations of Coarse-grained Proteins in Implicit Solvent. *J. Phys. Chem. B* **2009**, *113*, 267− 274.

(72) Yu, X.; Zheng, J. Polymorphic Structures of Alzheimer's β-Amyloid Hlobulomers. *PLoS One* **2011**, *6*, e20575.

(73) Zhao, J.; Hu, R.; Sciacca, M. F. M.; Brender, J. R.; Chen, H.; Ramamoorthy, A.; Zheng, J. Non-Selective Ion Channel Activity of Polymorphic Human Islet Amyloid Polypeptide (Amylin) Double Channels. *Phys. Chem. Chem. Phys.* **2014**, *16*, 2368−2377.

(74) Huang, S. M.; Abernethy, D. R.; Wang, Y.; Zhao, P.; Zineh, I. The Utility of Modeling and Simulation in Drug Development and Regulatory Review. *J. Pharm. Sci.* **2013**, *102*, 2912−2923.

(75) Wang, Q.; Zhao, C.; Zhao, J.; Wang, J.; Yang, J. C.; Yu, X.; Zheng, J. Comparative Molecular Dynamics Study of Aβ Adsorption on the Self-Assembled Monolayers. *Langmuir* **2010**, *26*, 3308−3316.

(76) Zheng, J.; Yu, X.; Wang, J.; Yang, J. C.; Wang, Q. Molecular Modeling of Two Distinct Triangular Oligomers in Amyloid β-Protein. *J. Phys. Chem. B* **2010**, *114*, 463−470.

(77) de Jong, D. H.; Singh, G.; Bennett, W. F. D.; Arnarez, C.; Wassenaar, T. A.; Schafer, L. V.; Periole, X.; Tieleman, D. P.; Marrink, S. J. Improved Parameters for the Martini Coarse-Grained Protein Force Field. *J. Chem. Theory Comput.* **2013**, *9*, 687−697.

(78) Zheng, J.; Ma, B.; Tsai, C. J.; Nussinov, R. Structural Stability and Dynamics of an Amyloid-Forming Peptide GNNQQNY from the Yeast Prion Sup-35. *Biophys. J.* **2006**, *91*, 824−833.

(79) Zhao, J.; Yu, X.; Liang, G.; Zheng, J. Structural Polymorphism of Human Islet Amyloid Polypeptide (hIAPP) Oligomers Highlights the Importance of Interfacial Residue Interactions. *Biomacromolecules* **2011**, *12*, 210−220.

(80) Miller, Y.; Ma, B.; Nussinov, R. Polymorphism of Alzheimer's Aβ17−42 (p3) Oligomers: the Importance of the Turn Location and its Conformation. *Biophys. J.* **2009**, *97*, 1168−1177.

(81) Wineman-Fisher, V.; Atsmon-Raz, Y.; Miller, Y. Orientations of Residues along the β-Arch of Self-Assembled Amylin Fibril-Like Structures Lead to Polymorphism. *Biomacromolecules* **2015**, *16*, 156− 165.

(82) Zhang, M.; Hu, R.; Chen, H.; Chang, Y.; Gong, X.; Liu, F.; Zheng, J. Interfacial Interaction and lateral Association of Cross-Seeding Assemblies between hIAPP and rIAPP Oligomers. *Phys. Chem. Chem. Phys.* **2015**, *17*, 10373−10382.

(83) Goldsbury, C. S.; Cooper, G. J. S.; Goldie, K. N.; Muller, S. A.; Saafi, E. L.; Gruijters, W. T. M.; Misur, M. P.; Engel, A.; Aebi, U.; Kistler, J. Polymorphic Fibrillar Assembly of human Amylin. *J. Struct. Biol.* **1997**, *119*, 17−27.

(84) Yu, X.; Luo, Y.; Dinkel, P.; Zheng, J.; Wei, G.; Margittai, M.; Nussinov, R.; Ma, B. Cross-Seeding and Conformational Selection between Three- and Four-Repeat human Tau Proteins. *J. Biol. Chem.* **2012**, *287*, 14950−14959.

(85) Siddiqua, A.; Luo, Y.; Meyer, V.; Swanson, M. A.; Yu, X.; Wei, G.; Zheng, J.; Eaton, G. R.; Ma, B.; Nussinov, R.; Eaton, S. S.; Margittai, M. Conformational Basis for Asymmetric Seeding Barrier in Filaments of Three- and Four-Repeat Rau. *J. Am. Chem. Soc.* **2012**, *134*, 10271−10278.

(86) Meyer, V.; Dinkel, P. D.; Luo, Y.; Yu, X.; Wei, G.; Zheng, J.; Eaton, G. R.; Ma, B.; Nussinov, R.; Eaton, S. S.; Margittai, M. Single Mutations in Tau Modulate the Populations of Fibril Conformers through Seed Selection. *Angew. Chem., Int. Ed.* **2014**, *53*, 1590−1593.

(87) Luo, Y.; Dinkel, P.; Yu, X.; Margittai, M.; Zheng, J.; Nussinov, R.; Wei, G.; Ma, B. Molecular Insights into the Reversible Formation of Tau Protein Fibrils. *Chem. Commun.* **2013**, *49*, 3582−3584.